2017

LNF Highlights

da qualche parte,
qualcosa di incredibile
è in attesa
di essere scoperto
(Carl Sagan)

29

INFN

Istituto Nazionale di Fisica Nucleare

Laboratori Nazionali di Frascati

One year

of Research

at LNF: 2017

Foreword

As usual, 2017 has been an intense year for the Laboratori Nazionali di Frascati and its staff.
DAΦNE has continued to provide beam to KLOE-2 throughout the whole year. The efficiency has been very high, and the peak luminosity has been well above 2×10^{32} cm^{-2}s^{-1}. This gives a great confidence in achieving the goal of collecting 5 fb^{-1} on tape by the end of March 2018. In the meantime, the preparation for the PADME and the SIDDHARTA2 experiments are well on track. The Laboratory is also thinking to guarantee a new life for DAΦNE, after 2020, when the collider mode will be terminated. A facility oriented to host accelerator physics and technology studies appears of interest for the European community.

The Laboratory is continuing the study for an infrastructure oriented to develop advanced technologies in particle acceleration for future linac colliders and for applied physics, within the EU-PRAXIA H2020 design study, an Executive Summary of the CDR, to present a first layout of the infrastructure and its cost, has been presented in summer to INFN, which has given green light for further studies and for the preparation of a full CDR. The project, based on X- band and plasma technologies, has also elicited the interest of CERN and ELETTRA accelerator communities.

LHC experiments and NA62 are collecting data at full speed, and LHCb is showing intriguing data pointing to possible violation of lepton universality. Only the analysis of the full data sample will give better confidence in the results. As well, construction of phase 2 upgrades are entering slowly in a steady-state regime. The CLAS12 experiment at JLAB has installed the large Cerenkov detector, fully engineered and built at LNF. New ideas on how to reuse the large DAΦNE magnets for very challenging searches of axions have been presented and discussed in the LNF community.

A long list of outreach activities has characterized 2017: Open Day, public lectures, matinees of science, training of high school students and teachers, etc..., with nearly 8,000 people visiting the premises. The efforts done on Technological Transfer show the strong commitment of the Laboratory to contribute to the Third Mission of INFN and to the development of local SMI.

Further young people have been hired and more will come in 2018. This is vital for the Laboratory, given the many new long-term projects and the need for fresh minds.

I acknowledge, with pleasure, the outstanding role of the whole LNF staff in achieving these results. To them all, my warmest and deepest thanks

Pierluigi Campana

LNF Director

Beauty hadrons at LHCb challenge the Standard Model

Since its birth, the Standard Model (SM) of particle physics has proven remarkably successful at describing experimental measurements, but despite its incredible accuracy, we know that the SM must be incomplete: it offers no explanation for the cosmological evidence of dark matter, nor does it account for the dominance of matter over antimatter in the Universe. The quest for what may lie beyond the SM is at the core of the LHC physics program: ATLAS and CMS systematically search for the direct production of beyond the Standard Model (BSM) particles, predicted by various extensions to the SM, while LHCb uses the complementary and quite elegant approach of observing the effects of yet undiscovered particles or other BSM physics in well-known SM processes. These effects are predicted to be small, so that the proposed new-physics extensions remain consistent with observations, but through the quirks of quantum mechanics quantum loops can appear in the diagrams describing SM decays, which get influenced by particles not present in their initial or final states. The high luminosity of LHC and the unprecedented precision of its experiments allow probing these putative effects at levels never reached in previous measurements.

This is the core field of study at LHCb, designed for precision measurements of CP violation and rare decays of beauty and charm hadrons. LHCb published more than 440 papers using mainly Run 1 (2010-2012) data, with some contributions also from the Run 2 (2015-2018). During the LHC Long Shutdown 1 (2013-2014) the LHCb detector remained essentially unchanged while an innovative trigger model has been put in place: thanks to the real-time alignment and calibration of the detectors, the online event reconstruction has the best offline quality and is used for most of the datasets, reserving offline reconstruction to few special physics cases. In the ongoing Run 2, LHCb successfully afforded many operational challenges and already col-

lected ~3.7 fb^{-1} (end of 2017) that sum up to the ~3 fb^{-1} collected in Run 1. A LHCb upgrade is scheduled, with installation in 2019-2020 (LHC LS2). The motivation is to take increased advantage of the huge rate of heavy-flavor production at LHC by means of a full software trigger, and raising the operational luminosity by factor 5 up to 2×10^{33}cm^{-2}s^{-1}. The LHCb Collaboration also issued an Expression of Interest in an LS4 Upgrade, for a High Luminosity LHC era flavor physics experiment. The LHCb Frascati group is deeply involved in all the ongoing activities, from data analysis to the R&D for the upgrades, having also important responsibilities both on the hardware and software side.

THE QUEST FOR THE $B_s^0 \rightarrow \mu^+\mu^-$ decay

The branching fraction of the B_s^0 meson to decay into two oppositely charged muons is very small in the SM and is very well predicted. On the other hand, a large class of theories that extend the SM, such as for example supersymmetry, allows for modifications to this branching fraction: an observation of any significant deviation from the SM prediction would indicate a discovery of new effects. The $B_s^0 \rightarrow \mu^+\mu^-$ decay has therefore long been regarded as one of the most promising reactions to search for these new effects. This decay has been searched for more than 30 years by different experiments at different accelerators. The LHCb collaboration obtained the first evidence [1], with a significance of 3.5 standard deviations, in November 2012 and, in February 2017, the first observation, by a single experiment, of the $B_s^0 \rightarrow \mu^+\mu^-$ decay, with a statistical significance of 7.8 standard deviations [2]. The measured branching fraction $(3.0\pm0.6^{+0.3}_{-0.2})$ x 10^{-9} is consistent with the SM prediction of (3.65 ± 0.23)x 10^{-9}[3]. The full 3 fb^{-1} of the data collected during Run 1, and 1.4 fb^{-1} of the data accumulated during Run 2 were used to obtain this result, the most precise measurement of this quantity to date.

The $B^0 \to \mu^+\mu^-$ decay, expected in the SM at a rate of about 30 times smaller than the $B^0_s \to \mu^+\mu^-$, it is not found to be significant and then an upper limit is set for the decay at a value of 3.4×10^{-10}. These results severely constrain the possible SM-extension models that are still allowed, and therefore focus future experimental searches and theoretical attention [4-5].
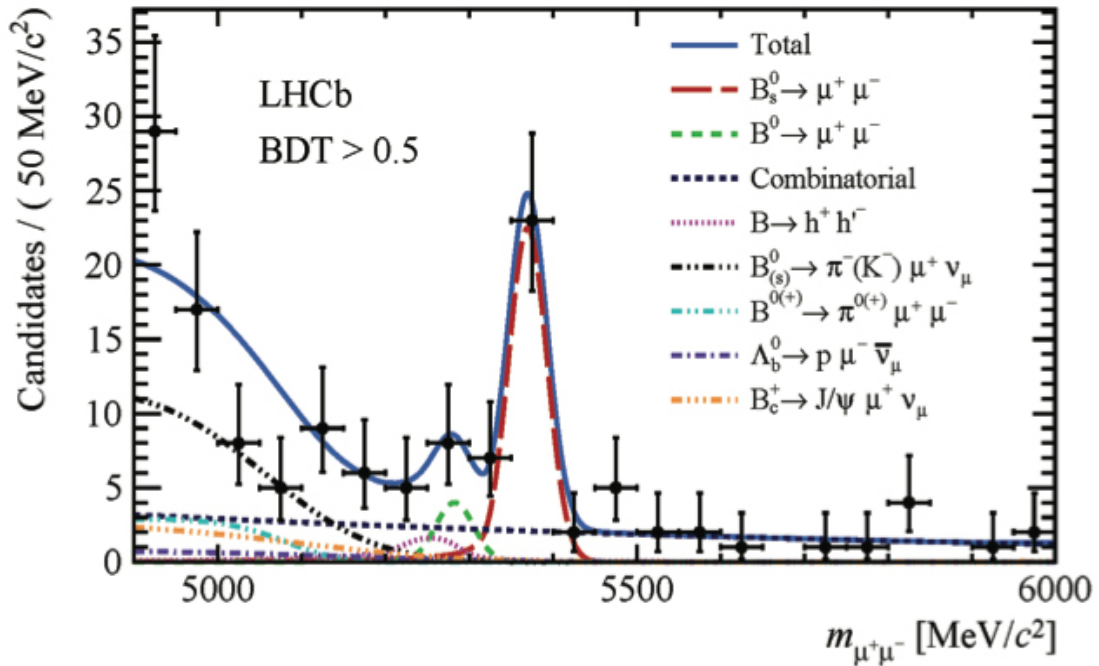
Figure 1 The $\mu^+\mu^-$ invariant mass spectrum for the bins with the smallest background contribution. The contribution of the $B^0_s \to \mu^+\mu^-$ decay is clearly visible at the B^0_s mass and is indicated as the red peaking distribution. The green peaking distribution shows a possible contribution of the $B^0 \to \mu^+\mu^-$ decay at lower mass. The other contributions show the background processes and provide very little contamination in the region of the $B^0_s \to \mu^+\mu^-$ signal.

Test of Lepton Flavor Universality

In the SM particles are organized into generations. The only known difference between them is the different strength of their interactions with the Higgs field, called Yukawa couplings. This results in different masses for each particle, giving a wide range of experimental signatures. For the charged leptons (e, μ, and τ), this implies a property known as Lepton Universality (LU): other than effects related to their different masses, all the SM interactions treat the three charged leptons identically. Recently, a series of measurements from B-factory and LHCb has tested the LU in many decay processes of beauty hadrons.

Hints of LU have been found and, even if none of the single results is significant on its own, all taken together point to the existence of non-SM forces or to phenomena that treat leptons differently depending on their flavor. If a deviation from LU was to be confirmed, it would be a clear evidence for physical processes beyond the SM. The results so far concern two classes of transitions in b-quark hadron decays: measurements of highly suppressed flavor-changing neutral-current (FCNC) processes, $b \to s\,\ell^+\ell^-$, hinting at a difference involving muons and electrons, and measurements of the more frequent tree-level processes, $b \to c\ell^+\nu_\ell$ hinting at a difference between muons and taus. The formers are highly suppressed because there are no tree-level FCNC in the SM. This suppression increases the sensitivity to the possible existence of new physics as the presence of new particles contributing to these processes could lead to a sizeable increase or decrease in the rate of particular decays, or change the angular distribution of the final-state particles. The observables are the ratio of branching
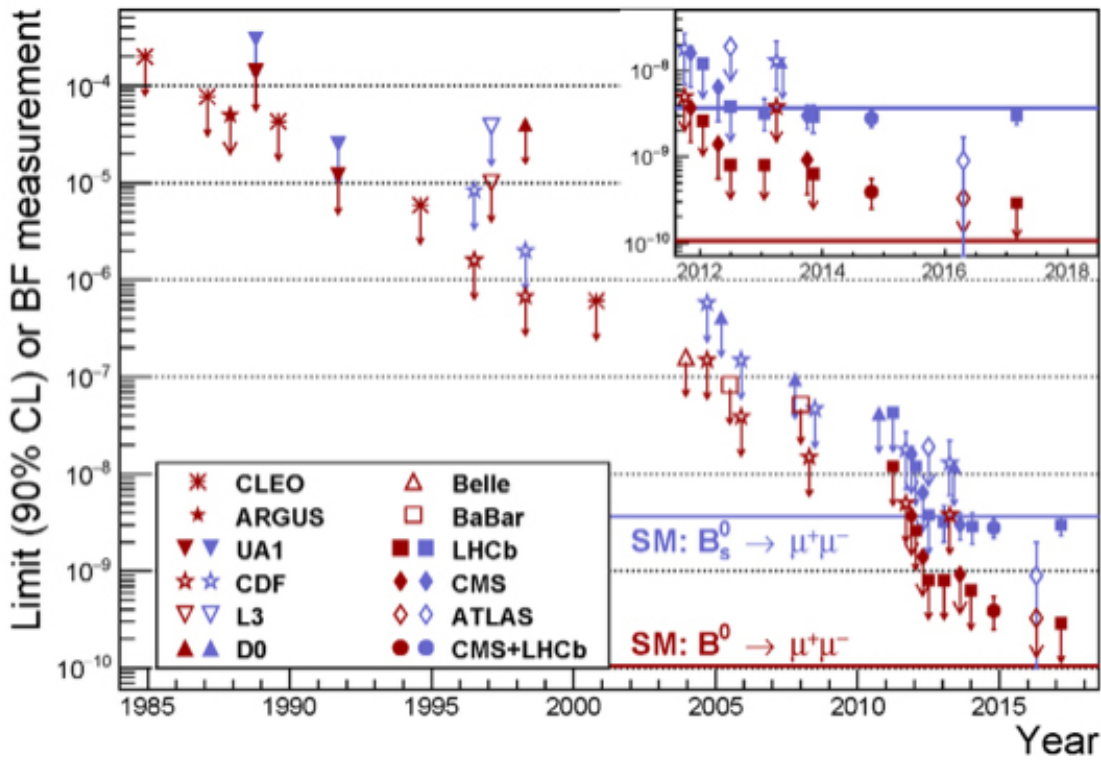
Figure 2 The $B_s^0 \to \mu^+\mu^-$ and $B^0 \to \mu^+\mu^-$ decays have been searched for more than 30 years by different experiments at different accelerators.

fractions between muon and electron decay modes , $R_{K^*} = BF(B \to K^*\mu^+\mu^-)/ BF (B \to K^*e^+e^-)$, differential branching fractions of decays like $B^+ \to K^+\mu^+\mu^-$, $B^0 \to K^0\mu^+\mu^-$ and $B_s^0 \to \varphi\mu^+\mu^-$, as well as the angular distribution of the decay products of the same decays. Experiments at B-factories, BaBar and Belle have measured R_{K^*} ratios and found them to be consistent, with a large uncertainty, with the SM. The LHCb measurements of R_{K^*} [6] and R_K [7] are more precise and all have a tendency to sit below the SM predictions.

For what concerns $b \to c_\ell^+ \nu e$ the tree-level processes, the quantities experimentally measured are the ratios of branching fractions $R_{D^*} = BF (B \to D^*\tau^+\nu_\tau)/ BF (B \to D^*\ell^+\nu_\ell)$, with $\ell = e$ or μ. Since the hadron effects, embedded in the $B \to D^*$ form factors, cancel a large extent in these ratios, the SM prediction for R_D and R_{D^*} are known with uncertainties of few percent level [8-9].

Experimentally, such semi-tauonic beauty decays are extremely difficult to measure because τ are not reconstructed directly and at least two undetected neutrinos are present in the final state. Values for R_D and R_{D^*} above the SM prediction were first measured by BaBar in 2012, followed in 2015 by results from Belle that were also consistently high. These measurements were deemed not feasible at hadronic colliders, but in 2015 LHCb released the first result on R_{D^*} at an hadron collider [10]. In this measurement the τ lepton was reconstructed into its decays into a μ and two neutrinos. The measurement was possible thanks to the overall excellent performance of the LHCb detector, with a pivotal role of the vertex locator. This measurement again came out higher than the SM prediction, thus strengthening the tension between theory and experiment raised by Belle and BaBar. In 2017, LHCb presented another measurement [11, 12] by exploiting the decay of the τ lepton into three charged pions and a neutrino, finding a value larger than, even if still compatible with, the SM expectations and consistent with previous determinations.

Tree-level and FCNC decays are sensitive to new physics at the O(TeV) and O(10 TeV) level, respectively, and a model that can explain both kinds of anomalies seems difficult to find, nevertheless recent theoretical developments are captivating. Experimentally it is important to increase the accuracy of all the above results and also to look for the same anomalies in studying the decay of other b-hadron species. All the LHCb measurements aiming at testing the LU have been performed using data from Run 1 only.

New results, exploiting also Run 2 data, are expected over the coming months, as well as the measurement of the $R_{D_S^*}$ ratios. If these hints of LU would be confirmed by other measurements, it will clearly be a sign of BSM physics and will enforce the need of LHCb future upgrades to accurately measure the properties of the new BSM particles or interactions.
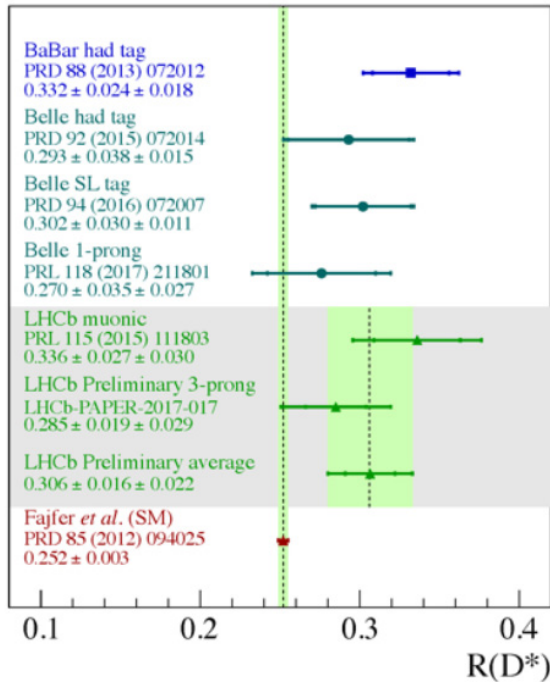
Figure 3 Comparison of different measurements of R_{D^*}. Different experiments operating either at pp (LHCb) or e$^+$e$^-$ (BaBar, Belle) colliders, using very different experimental techniques, measure values systematically above the SM prediction. The discrepancy between the experimental world average and the SM prediction is about 3.4 standard deviations.

References:
[1] LHCb Collaboration, Phys. Rev. Lett. 111, 101805 (2013).
[2] LHCb Collaboration, Phys. Rev. Lett. 118, 191801 (2017).
[3] C. Bobeth, M. Gorbahn, T. Hermann, M. Misiak, E.Stamou, and M. Steinhauser, Phys. Rev. Lett. 112, 101801 (2014).
[4] K. S. Babu and C. F. Kolda, Phys. Rev. Lett. 84, 228 (2000).
[5] G. Isidori and A. Retico, J. High Energy Phys. 11, 001 (2001).
[6] LHCb Collaboration, J. High Energy Phys. 08, 055 (2017).
[7] LHCb Collaboration, Phys. Rev. Lett. 113, 151601 (2014).
[8] S. Fajfer, J. F. Kamenik, and I. Nisandzic, Phys. Rev. D85, 094025 (2012).
[9] D. Bigi and P. Gambino, Phys. Rev. D94, 094008 (2016).
[10] LHCb Collaboration, Phys. Rev. Lett.115, 111803 (2015).
[11] LHCb Collaboration, Phys. Rev. Lett. 120, 171802 (2018).
[12] LHCb Collaboration, Phys. Rev. D 97, 072013 (2018).

Search for Physics beyond the Standard Model at CERN: The NA62 Experiment

Figure 1 Picture of the NA62 experimental hall.

The Branching Ratio (BR) for the decay $K^+ \rightarrow \pi^+ \nu \bar{\nu}$ can be related to the value of the CKM matrix element ν_{td} with minimal theoretical uncertainty, providing a sensitive probe of the flavor sector of the Standard Model. The goal of the NA62 experiment at the CERN SPS is to detect ~100 of such decays with a S/B ratio of 10:1 (Fig. 1).
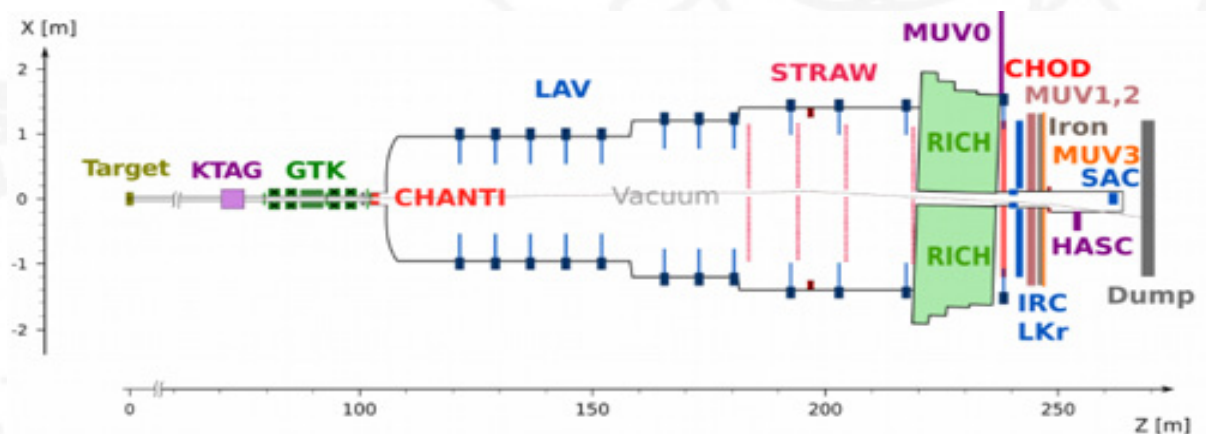
Figure 2 The NA62 experimental layout (see text for more details).

The experiment (Figs. 1 and 2) makes use of a 75 GeV unseparated positive secondary beam. The total beam rate is 800 MHz, providing ~50 MHz of K^+'s. The decay volume begins 102 m downstream of the production target. 5 MHz of kaon decays are observed in the 60 m long fiducial vacuum decay region. Ring-shaped large-angle photon vetoes (LAVs) are placed at 12 stations along the decay region and provide full coverage for decay photons with 8.5 mrad $< \theta <$ 50 mrad. The last 35m of the decay region hosts a dipole spectrometer with four straw-tracker stations operated in vacuum. The NA48 liquid-krypton calorimeter (LKr) is used to veto high-energy photons at small angle. Additional detectors further downstream extend the coverage of the photon veto system (e.g. for particles traveling in the beam pipe).

The LAV system consists of 12 detector stations arranged at intervals of 6 to 10 m along the vacuum tank along its entire length. The first 11 stations are incorporated into the tank itself and operate in vacuum. Each station consists of four or five rings of blocks, with the blocks staggered in azimuth in successive rings. The total depth of a five-layer station is 27 radiation lengths. This structure guarantees high efficiency, hermeticity, and uniformity of response. The entire LAV system is under the LNF responsibility [1]. NA62 took its first physics data in 2016. During the 2016 run, most data was taken with the beam intensity at 40% of nominal intensity, because of limitations by the quality of the SPS slow extraction. A sample of 5×10^{11} kaon decays in the 60 m long fiducial volume was collected. This data set was used to perform a first analysis of $K^+ \rightarrow \pi^+ \nu \nu$. The analysis of these data was performed using a blind procedure, with signal and control regions kept masked until the evaluation of expected signal and background was complete. The preliminary result has been presented at the Moriond EW conference and in a dedicated seminar at CERN [2].
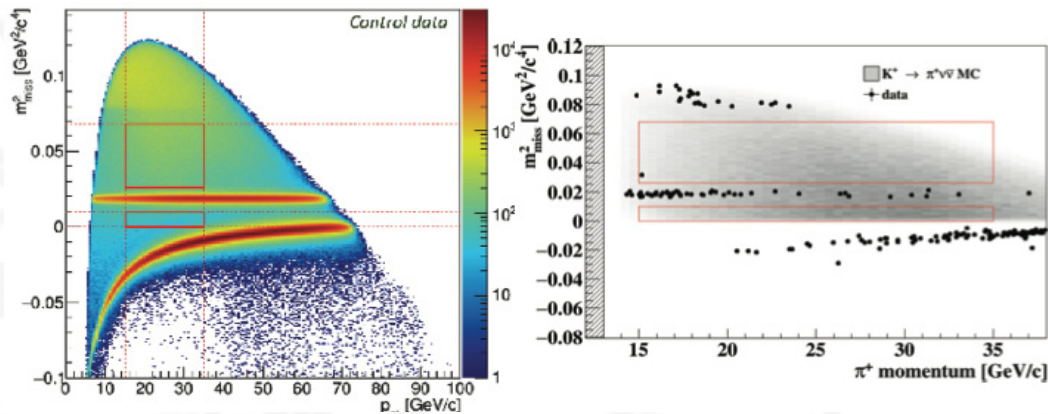
Figure 3 (left) m^2_{miss} as a function of momentum P_π after K^+ decay selection. Red boxes define the signal regions. (right) m^2_{miss} as a function of P_π momentum after all cuts except the m^2_{miss}. The event observed in region 2 is shown. Grey area represents $K^+ \rightarrow \pi^+ \nu \bar{\nu}$ MC events distribution

The analysis is mostly cut based. The goal is to reach the single-event sensitivity for $K^+ \rightarrow \pi^+ \nu \bar{\nu}$ at the SM BR and to exercise the background rejection capabilities of NA62. The selection proceeds through definition of K^+ decays with a charged particle in the final state, π^+ identification, rejection of events with a π^0 or any other activity in final state, kinematic selection, and definition of the signal regions. The π^0 rejection is an important ingredient in the analysis, and the LNF team, which is responsible for the photon veto system, has made critical contributions. The kinematic selection is based on the missing mass variable m^2_{miss}. The distribution of selected K^+ decays in the (m^2_{miss}, P_π) plane is shown in Fig. 3. Regions populated by $K^+ \rightarrow \pi^+ \pi^0$ (γ), $K^+ \rightarrow \mu^+ \nu$ (γ), and $K^+ \rightarrow \pi^+ \pi^- \pi^+$ are visible. Two signal regions are defined: the region at lower (higher) m^2_{miss} is referred to in the text as region 1 (2). The m^2_{miss} resolution, 10^{-3} GeV^2/c^4 at the $K^+ \rightarrow \pi^+ \pi^0$ peak, drives the choice of the boundaries of these regions. After the application of all signal selection cuts and the evaluation of the expected background, the signal regions are opened, and one event is found in region 2, Fig. 3 (right). In this event, the secondary track has a momentum of 15.3 GeV/c and the RICH clearly indicates that it is a pion. The expected background is 0.15 ± 0.09stat ± 0.01syst. A preliminary upper limit on the branching ratio of the $K^+ \rightarrow \pi^+ \nu \bar{\nu}$ decay is derived from this result using the CLs method: $BR(K^+ \rightarrow \pi^+ \nu \bar{\nu}) < 14 \times 10^{-10}$@95% CL. The expected number of signal events at the SM BR is 0.27 ± 0.01stat ± 0.02 syst ± 0.03 ext. The 2017 run was very successful. About $3 \times 10^{12} K^+$ decays were collected. Data taking took place at an average beam intensity close to 60% of nominal. Lower than nominal intensity is justified by the need for stable data taking with high efficiency. The analysis of the 2017 data is underway. On the basis of the statistics collected in 2017 and the ones expected in 2018, NA62 should be able to observe about 20 $\pi^+ \nu \bar{\nu}$ SM events, providing a 20% measurement of the branching ratio with data taken by the end of 2018.

References:
[1] A. Antonelli, http://www.lnf.infn.it/rapatt/2017/na62.pdf
[2] G. Ruggero, https://indico.cern.ch/event/714178/

A new eye to study the nucleons electron conversion experiment

Protons and neutrons (or nucleons) constitute more than 99% of the visible matter of the universe. They are made up by more elementary constituents, quarks and gluons, whose interaction is described by the Quantum Chromo Dynamics (QCD).

The nucleons are complex objects and even their more basic properties are very difficult to be described within the QCD. For example, while the Higgs mechanism can explain the origin of the mass of the quarks, only about 1% of the nucleon mass originates from the constituents that determine their charge and baryon number. The remaining 99% originates from interaction energy involved in the QCD mechanisms that lead to confinement, which is a highly nontrivial problem to solve. Properties of the nucleons that are still not well understood are also the spin and its decomposition in terms of the basic constituents and the excitation spectrum. One of the best ways to experimentally study the nucleon structure is through scattering of high energy, highly polarized electrons on targets of hydrogen or heavier nuclei. The detection of specific particles in the final state opens a window into the contribution to the nucleon properties of quarks and gluons of different flavors: pions are generally used to pin down the valence up and down quarks, kaons for strange sea quarks, heavier particles like the J/ψ for the gluons.

The study of the nucleon structure with electron beams is one of the main items of the physics program carried out in the experimental Hall B of the Thomas Jefferson National Accelerator Facility in Newport News (Virginia, USA). Here, the unique electron beam of the Continuous Electron Beam Accelerator Facility, with maximum energy of 11 GeV, polarization bigger than 80% and luminosity of the order of 10^{35} cm^{-2} s^{-1}, is used with the CLAS12 spectrometer, which is able to detect multi-particle final states with large geometrical acceptance. In January 2018, the first of two modules of a
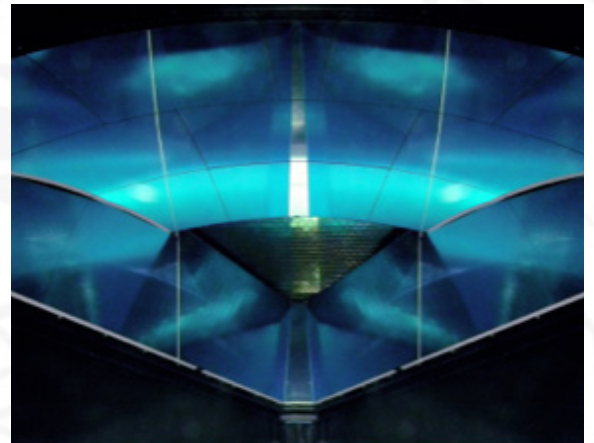
Figure 1 View of the interior of the CLAS12 RICH, with the spherical and lateral planar mirrors and the MAPMT array.

new Ring Imaging CHerenkov (RICH) detector (Fig. 1), designed and built under the lead of INFN researchers, has been installed in the CLAS12 spectrometer. The RICH exploits the highly directional light emitted by particles that travels in transparent media with speed higher than that of the light in the medium (the so-called Cherenkov effect). The emission angle depends on the refractive index of the medium and on the particle's speed: the higher is the speed, the smaller is the angle. Thus, the measurement of the emission angle provides the particle's mass (if its momentum is known) and therefore allows its identification. The CLAS12 RICH has been designed in order to discriminate kaons from pions and protons in the momentum range from 3 to 8 GeV/c. The detector design has been challenging in many aspects. The dimensions (about 4.3 m height and 4.1 m width) required accurate simulation studies to keep the area to be instrumented within reasonable size thus reducing the costs. The result of these studies has been a hybrid geometry, in which the photons can be detected either directly after their emission or after reflection on a mirror system. In addition, being in the acceptance of the CLAS12, it has to be light to minimize the influence on the other components of

the spectrometer, but also extremely rigid, to guarantee the necessary angular resolution in the detection of the Cherenkov photons. This has been achieved by extensively using light materials, like aluminum and carbon fiber, and the sandwich construction technique, in which two thin layers of material are glued to a thick honeycomb core, obtaining excellent rigidity also for elements of the dimension of several meters. The chosen radiator is silica aerogel, produced in large tiles of 20x20 cm^2 and thickness of 20 and 30 mm, the latter being the biggest aerogel tiles ever used in physics experiments. The laboratory tests demonstrated high optical quality at a refractive index (n=1.05) never reached in the aerogel used in other particle detectors. The aerogel is assembled on the entrance panel of the RICH (Fig. 2). A special system has been developed in order to keep the tiles in place when the RICH is assembled in its vertical position in CLAS12. he mirror system covers several squared meters of surface and includes seven planar glass mirrors and 10 carbon fiber spherical mirrors (Fig. 1). Both the glass and carbon fiber mirrors imply the sandwich technique to reduce the material budget. Particularly innovative are the two frontal planar mirrors, which use extremely thin glass layers of 0.7 mm thickness, never used in particle or space physics experiments.

The Cherenkov photons are detected on an array of 391 Multi-Anode Photo-Multiplier Tubes (MAPMTs), see Fig. 1. Each MAPMT is a matrix of 8x8 pixels, each pixel having a square 6x6 mm^2 area.
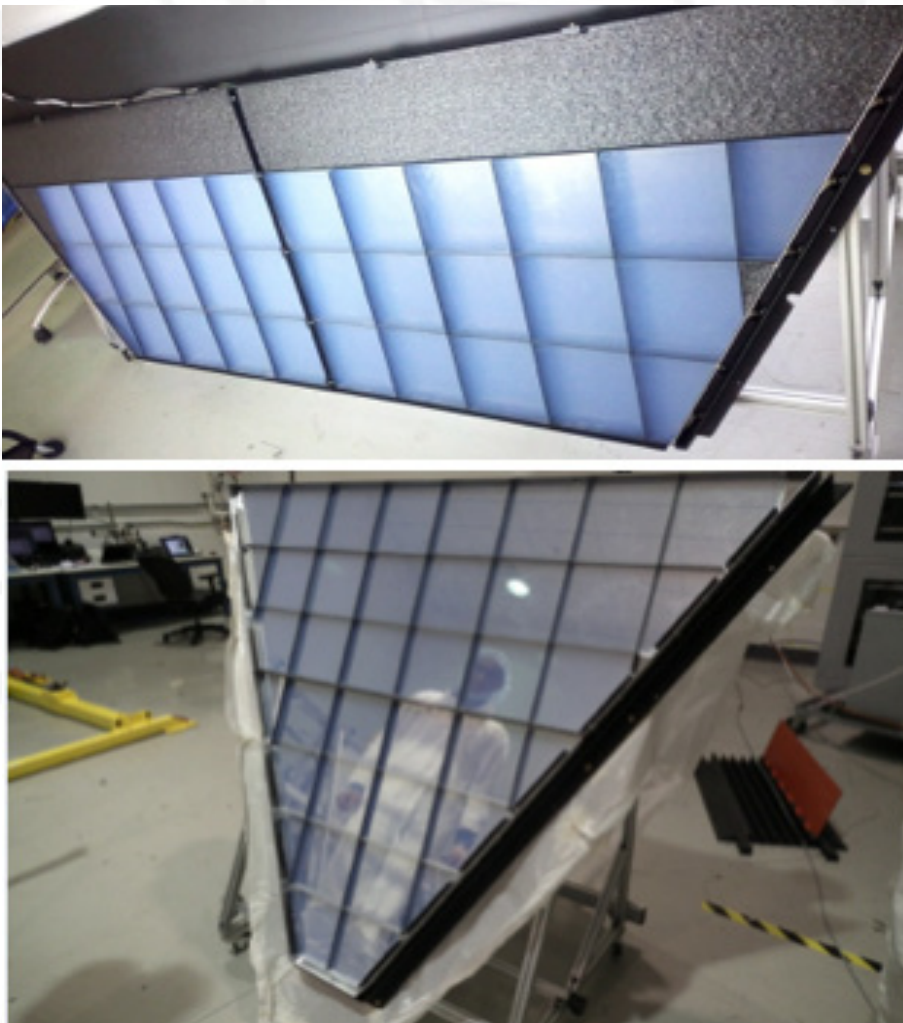
Figure 2 The two aerogel sections: the one with two layers of 30 mm thickness (top) and the one with one layer of 20 mm thickness (bottom).
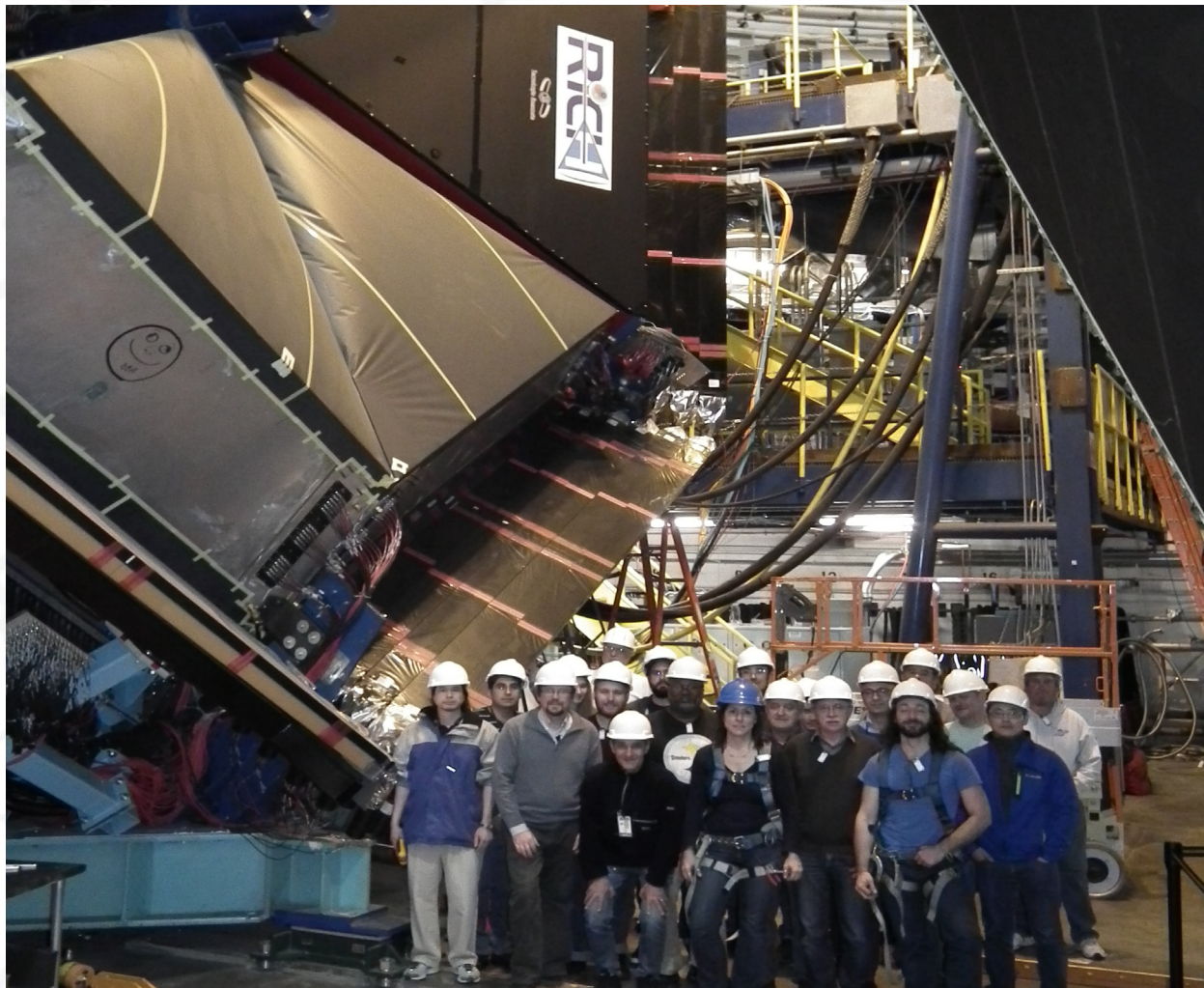
Figure 3 The RICH installed in CLAS12

The total number of readout channels is 25024. The Front-End electronics, installed on the back of the MAPMT array, is based on the MAROC3 chip, which provides a fast binary line with an adjustable preamplifier, a highly configurable shaper and a discriminator with adjustable threshold. A specially designed Field Programmable Gate Array (FPGA) with optical link is used to configure and readout the MAROC3 chips.

The construction of the RICH involved physicists, technologists and technicians of many INFN sections and foreign Institutions, under the lead of the Frascati and Ferrara physicists. The project also won a "premiale" funding from the Italian Ministry for the University and the Research.

The assembly and installation of the first RICH module have been carried out during several months in 2017 (Fig. 3). Finally, in January 2018 the data taking started and the first events have been recorded (Fig. 4).
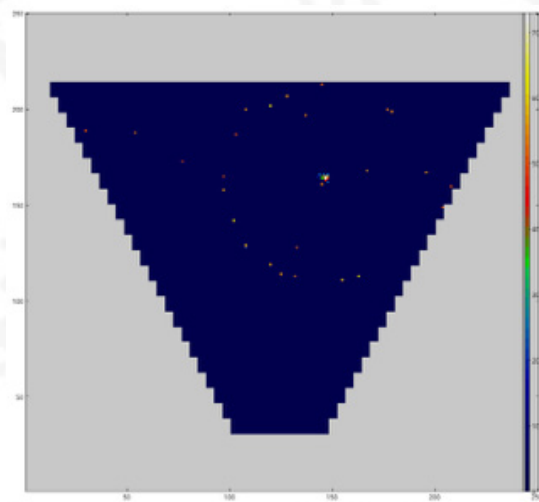
Figure 4 One of the forst RICH events, with a clear Cherenkov photon ring.

Terahertz and mid-infrared plasmons in three - dimensional nanoporous graphene

Graphene is the first thermodynamically stable two-dimensional material found in nature. Its properties are extraordinary: from high electrons mobility based on its linear dispersion (Dirac electrons), to strong interaction with the electromagnetic field, high thermal conductivity and high mechanical hardness.

In recent years, research has focused on providing a third dimension in graphene. Recently, three-dimensional graphene materials have been discovered (3D) with micro and nano-porous structures, or consisting of mesoscopic filaments that are distributed over macroscopic length scales. These topological structures help to preserve the extraordinary electrical properties and thermodynamic properties of 2D graphene extending the three-dimensional world.

The porous or filamentous nature and the high surface / volume ratio of these 3D architectures open up interesting applications and fundamental physics scenarios: from superconductivity, for batteries and supercapacitors uses, flexible electronics, photonics up to infrared and terahertz and plasmonics.
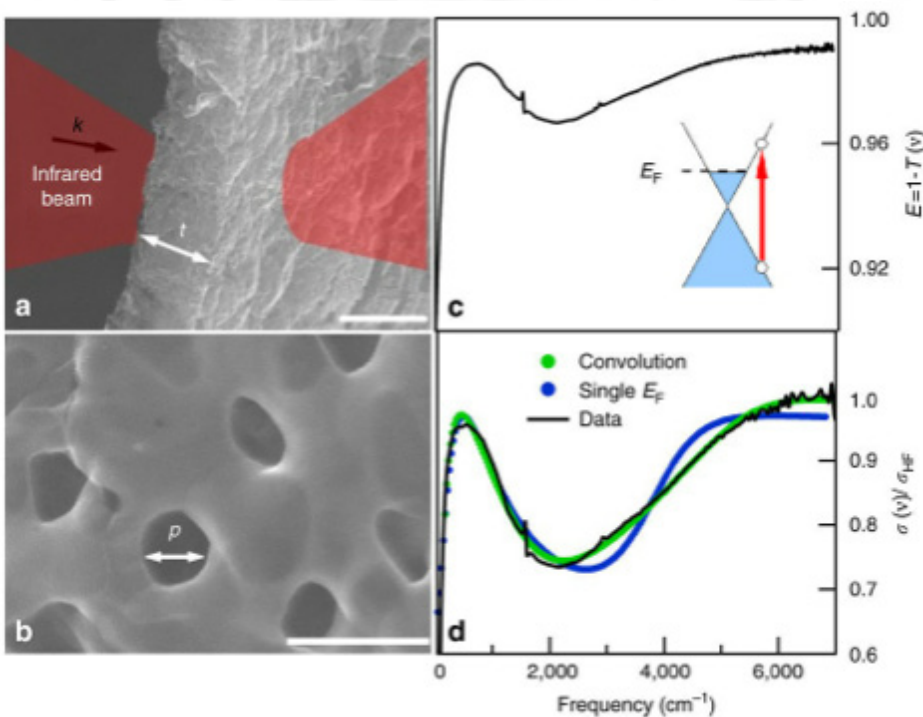
Figure 1 Nanoporous graphene structure and optical results. SEM images at lower (a) and higher (b) magnifications of a NPG sample with a thickness t=10±1 mm and average pore size p=200±50 nm. Scale bars correspond to 10 mm and 500 nm for (a,b) respectively. In (a) we also show the optical transmittance measurement scheme. (c) Typical extinction spectrum exhibits, at high frequency, a saturated absorption and, at low-frequency, a plasmonic broad peak separated by the Pauli-Blocking minimum. In the inset of (c) we show schematically a Dirac interband transition (red arrow). (d) Optical conductivity as extracted from extinction data (c), by a Kramers-Kronig consistent fit, normalized to its high-frequency value (black solid curve) compared to models with a single (blue solid curve) and distributed (green solid curve) Fermi energy.

These electromagnetic properties have been studied recently through a collaboration between the IIT @ Sapienza, the INFN-LNF and the TERALAB laboratory of the Physics Department of La Sapienza [1].

3D nanoporous graphene structures show plasmonic absorption modes modulated by the terahertz region of the electromagnetic spectrum up to the mid-infrared, which have been measured at the Infrared beamline of the Synchrotron laboratory DAFNE Light.

These plasmonic modes, which appear as a result of the porous structure of the 3D graphene, maintain the peculiarities dictated by the nature of the Dirac electron 2D graphene moving with high mobility in the highly interconnected structure of the nanoporous graphene. The large surface / volume ratio, the low toxicological impact of graphene and the ability to confine molecules and biomedical materials in conjunction pores with nature "broad band" of the absorptions 3D plasmonic allow to obtain bio-compatible, economic and versatile sensors. A typical extinction spectrum $E(\nu)=1-T(\nu)$ of a nanoporous graphene (NPG) sample having an average porous size $p=200\pm50$ nm and a thickness $t=10\pm1\mu m$ is reported in Fig. 1c.

In micro- and nano- ordered structures based on conventional metals and 2D electron gas systems, the plasmon frequency depends on both the charge-carrier density (Fermi Energy) and the geometrical parameters of the structure (pore size). In a disordered system one still expects a dependence on these parameters, although disorder may affect the plasmon frequency, linewidth and intensity.

In Fig. 2 we show the SEM images of samples having the same average porosity ($p=200\pm50$ nm) and thickness ($t=10\pm1$ μm), versus an increasing Fermi energy. The corresponding optical conductivity normalized to its high frequency value is plotted in the right panels. The Fermi energy values were obtained from fitting to the experimental optical conductivity and correspond well to the values provided by independent measurements on samples from the same batch. The whole fit, the plasmon, and the interband components are represented by blue-dashed, bluedotted and green-dotted lines, respectively. When E_F increases towards higher energies (from e to h), the plasmon peak is blue shifted. This is expected when the car-
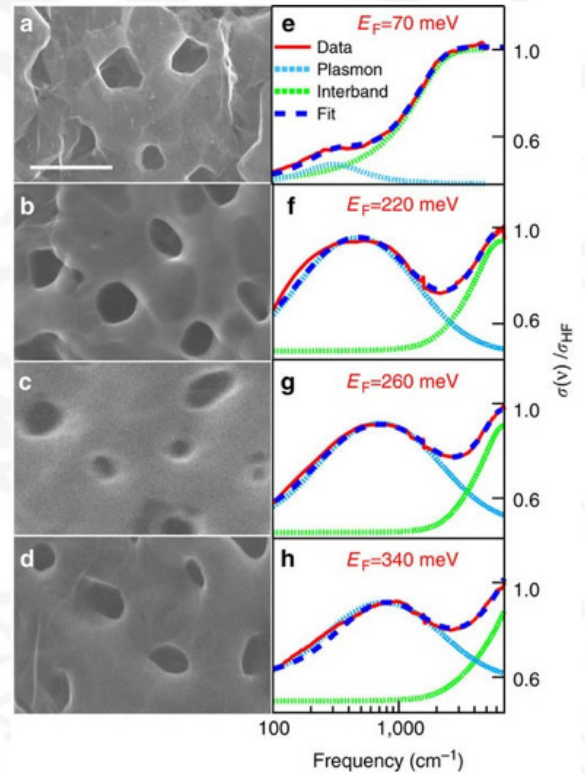
Figure 2 Optical properties of nanoporous graphene at fixed pore size for different Fermi energies. (a-d) SEM images of nanoporous graphene samples with the same average pore size $p=200\pm50$ nm, and an increasing Fermi energy. The scale bar corresponds to 500 nm. (e–h) Optical conductivity curves with relative value of Fermi energy. The whole fitting, the plasmon and the interband components (see text) are represented by blue-dashed, blue-dotted and green-dotted lines, respectively.

rier density increases due to a stiffening of the plasmonic restoring force.

The plasmon frequency ν_{pl} versus EF as obtained from fitting of data in Fig. 2, is reported in Fig. 3 (red squares). The error bars have been estimated through a statistical analysis on several samples having, nominally, the same properties. ν_{pl} clearly increases with EF passing from nearly 60 cm^{-1} for EFB70 meV to about 800 cm^{-1} for the highest doped N-NPG sample with $E_F=340$ meV. The good comparison among experimental data, theoretical fit and literature reports suggests that, although we are dealing with a disordered 3D structure, the plasmon excitation in NPG and N-NPG preserves a 2D Dirac character. This indicates further that plasmonic modes in NPG and N-NPG graphene represent the natural extension in 3D of Dirac plasmons in single-layer/few-layers graphene.

In conclusion, this work represents a systematic optical investigation of 3D nanoporous structures made of high-quality single-layer graphene. The optical conductivity of this nonperiodic array of graphene nano- and micro-pores exhibits both single-carrier interband transitions and collective plasmonic modes resonating at Terahertz and Mid-Infrared frequencies.

The plasmonic excitation depends both on doping and on the nanostructure geometry, the latter providing the extra-momentum needed to activate the radiation absorption process. The plasmon frequency dependence on the charge-carrier density (parametrized in terms of the Fermi energy), and pore size are in good agreement with a 2D Dirac character of plasmonic excitations in the 3D architecture of nano-porous graphene.

This suggests that the extreme wavelength-compression and field enhancement of graphene plasmons is at work. Furthermore, for N-doped samples, the microscopic inhomogeneity of doping and pore sizes yields a macroscopic plasmonic response that covers a wide spectral range (41,000 cm^{-1}). By taking into account the enhanced surface area of nanoporous structures, the tunability of graphene plasmon and the broad spectral response, the use of 3D NPG could pave the way for novel and competitive graphene based plasmonic-sensors.
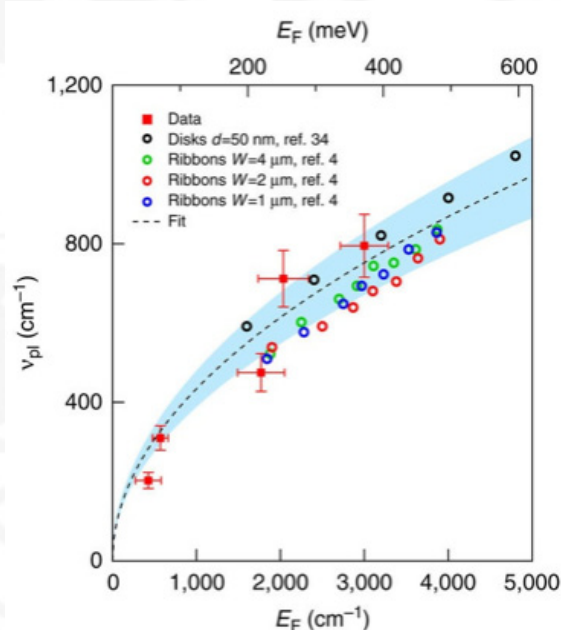
Figure 3 The plasmon frequency versus the Fermi energy. Data (red square markers) are compared with a fit based on Dirac two-dimensional (2D) plasmon frequency equation (equation (2), black dashed line). The shaded blue area represents the effect of parameter variation on the fit.

References:
[1] F. D'Apuzzo, A. R. Piacenti, F. Giorgianni, M. Autore, M. Cestelli Guidi, A. Marcelli, U. Schade, Y. Ito, M. Chen, and S. Lupi, Nature Com, 8:14885, DOI: 10.1038/ncomms14885 (2017).

Laser-matter interactions: ultra-fast evolution of electromagnetic pulses

The interaction of high-power ultra-short laser pulses with materials offers fascinating wealth of transient phenomena which are in the core of novel scientific research. Deciphering its evolution is a complicated task that strongly depends on the details of the early phase of the interaction, which act as complex initial conditions. The entire process, moreover, is difficult to probe since it develops close to the target on a sub-picosecond timescale and ends after some picoseconds.

At SPARC_LAB we measured the fields and charges generated by the interaction of the ultra-short high-intensity FLAME laser [1] with solid targets. The measurements have been carried out in a recent experimental campaign aimed to measure, with ultra-high temporal resolution, the phenomena related to the transfer of energy from a laser pulse to the matter [2]. A complete picture of all the processes involved in the laser-target interactions is experimentally complicated to obtain since different diagnostic techniques are usually needed.
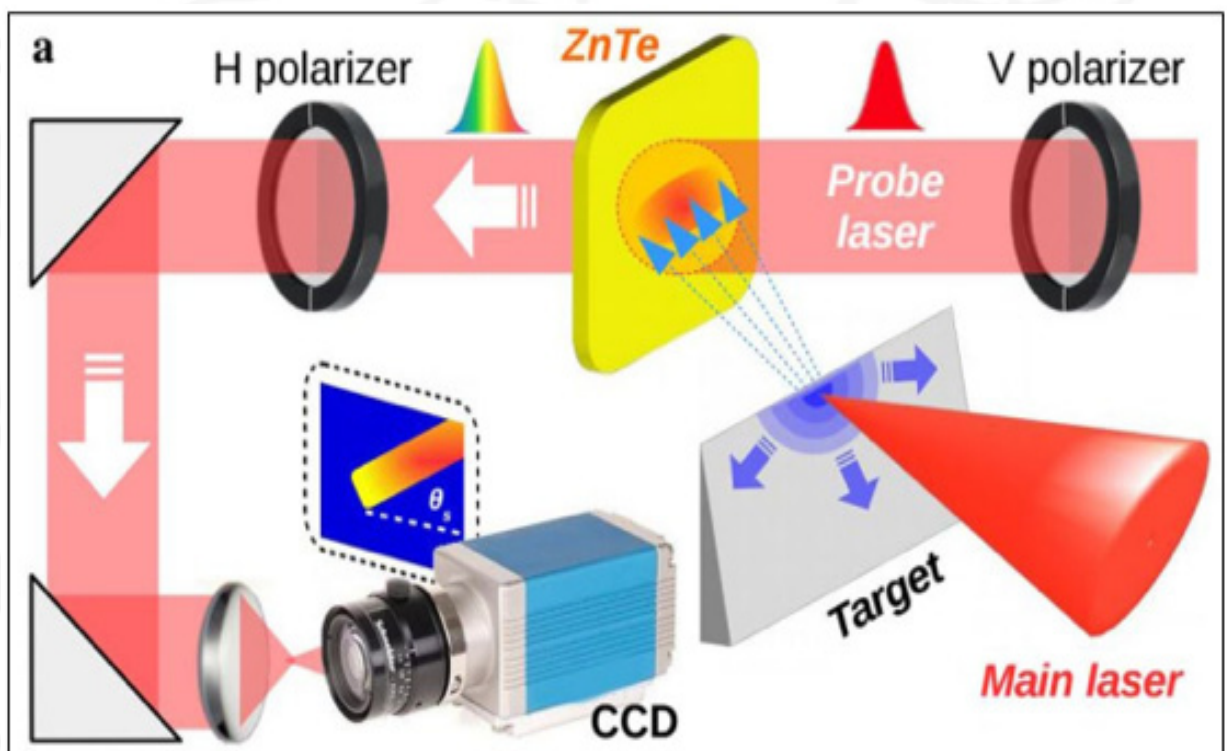
Figure 1 Experimental setup (see text for more details).

When a laser pulse operating at relativistic intensities (1018 W/cm^2) irradiates a solid target, a force driven by the laser field is produced and accelerates electrons up to relativistic velocities. These hot electrons propagate through the target and then are ejected. Some of them (fast electrons) are energetic enough to completely escape the target charging it rapidly. The unbalanced positive charge left on the target leads to the formation of a strong electric potential that locks the majority of hot electrons close to the target.
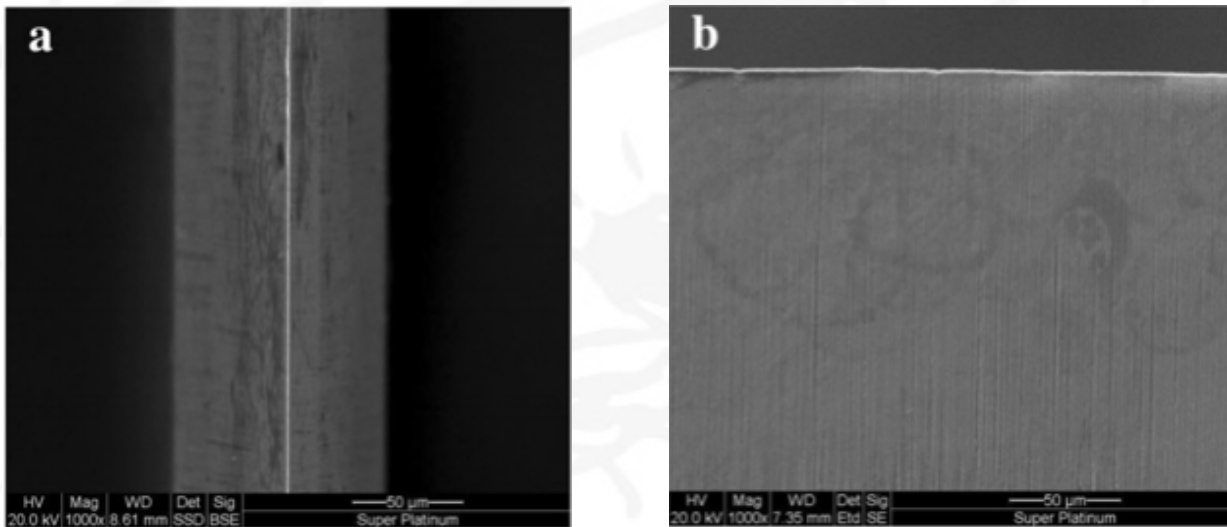
Figure 2 Top (a) and front (b) view of the razor blade used in the experiment

The hot electrons bounce back and forth and continue to ionize the matter creating a plasma. Such a re-circulation generates huge electromagnetic pulses, up to some Teravolt per meter (TV/m) depending on the laser intensity, consisting of ultra-short electromagnetic pulses emitted in the THz domain [3].

Figure 1 shows the experimental setup developed on the experimental chamber of the FLAME laser facility.
The laser, with intensity IL $\approx 10^{18}$ W cm^{-2}, is focused on a stainless steel sharp target (0.7 μm-thick commercial razor blade, see Fig. 2). The temporal diagnostics is based on the Electro-Optical Sampling (EOS), i.e. on the electro-optic effect induced into a non-linear crystal (that becomes birefringent) by an externally applied electric field [4]. Such a birefringence is able to modulate the polarization of an incoming laser pulse impinging onto the crystal proportionally to the electric field amplitude. Our system employs a 10×10 mm^2 ZnTe electro-optic crystal (500 μm-thick) and a 35 fs probe laser derived from the main system. The probe laser enters into the ZnTe crystal with an incidence angle $\theta_i = 28°$ and realizes a spatial encoding of the temporal profile of the EM pulse along the probe transverse profile. An optical delay-line is used to change the timing of the probe with respect to the main laser in order to monitor the interaction at different times. The probe laser is finally detected by a CCD camera.

The interaction of intense short laser pulses with solid targets results in a strong heating of the interacting particles.
As a consequence, some high-energy electrons are ejected while others spread and dissipate their energy inside it. The entire process is directly correlated to the intensity of the interacting laser pulse and can be described in terms of the average temperature of the ejected hot electrons that, in our experimental conditions, is expected to be $T_h \approx 500$ keV.
Figure 3 shows the resulting signals coming from the laser-target interactions. The long cigar-shaped one represents the THz electromagnetic pulse emitted. In such a snapshot the escaping electrons are also clearly visible, highlighting two distinct components at different energies and charges [5]. The magnitude of the radiation pulse impinging onto the EOS crystal is retrieved by quantifying the amount of birefringence induced into the ZnTe crystal and sampled by the probe laser. We have measured electric fields up to 0.8 MV/m in our setup, corresponding to approximately 0.7 TV/m of peak fields in correspondence of the metallic target. We have also provided their temporal evolution by analyzing the temporal profile at different experimental conditions.
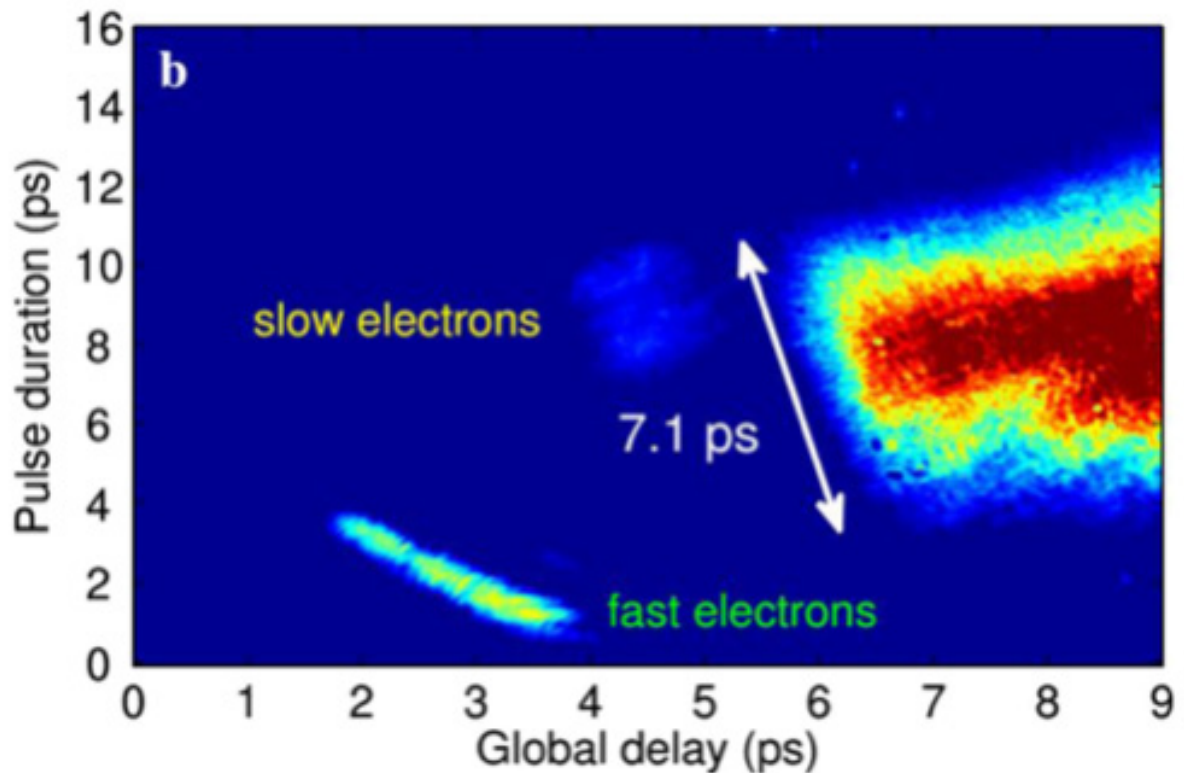
Figure 3 Electro-optic signal obtained by focusing the FLAME laser (2 J energy) onto the metallic target.

In conclusion, we provided femtosecond resolution measurements that allow operating on the same time scale of the process, determined by the duration of the driving laser pulse. In our experiment we observed the temporal evolution of the electromagnetic pulses emitted from metallic targets after the interaction with a high-intensity short pulse laser. Their lifetime of the order of several picoseconds with amplitudes of the order of 0.8 MV/m in correspondence of the EOS crystal. From this value we have inferred a field strength of approximately 0.6 TV/m on target, in agreement with PIC simulations. The provided snapshots also detected the forerunner fast particles that escaped from the target and offer a more complete physical picture of the entire interaction process. Our study opens the way to perform many new time-resolved experiments with the aim of achieving a closer and more complete vision of the phenomena involved in laser-matter interactions.

References:
[1] F. G. Bisesto et al., "The FLAME laser at SPARC_LAB", arXiv:1802.00398, submitted to Nucl. Instr. and Meth. A.
[2] R. Pompili et al., Scientific Reports 6, 35000 (2016).
[3] R. Pompili et al., Scientific Reports 8, 3243 (2018).
[4] R. Pompili et al., Opt. Express 24, 29512–29520 (2016).
[5] A. Curcio et al., Phys. Rev. App. 9.2, 024004 (2018).

LNF Outreach Activity

Figure 1 Visitors at LNF during the OpenLabs.

In 2017 LNF hosted a wide range of educational activities, both on and off site, for about 11000 participants from all over Italy and abroad.

OpenLabs is the most relevant of these activities. This year, "Playing with Science" welcomed more than 2500 participants. The program featured guided tours of the open experimental sites, conferences, interactive labs, video projections and scientific speed dates.

The event was organized in collaboration with LNF researchers, technologists, technicians and administrative personnel, and with the extra support provided by an additional staff of 70 high school students.

Amongst the various LNF educational activities we would point out those dedicated to the little ones. Actually, the Frascati National Laboratories has been contributing to the growth of the interest of young generations in particle physics for decades, in particular with the *Io dico l'Universo* program, addressed to both primary and lower secondary schools, which includes: guided tours of LNF, meetings with a researcher at LNF, but at schools and public libraries too.

Over the current school year, we have hosted over 800 students!

We welcomed a large crowd of little enthusiasts also at *OpenLabs*, during which activities beyond conventional teaching were scheduled and kids experienced physics playing with our researchers.

Furthermore, for the first time, LNF organized a special day of orientation – in terms of both university and job – with regard to STEM careers. *Our Visit & Career Day* – realized in collaboration with representatives of the world of Research, University and Industry – was a great success, involving more than 500 students from all over Italy.

Again this year, LNF proposed *Incontri di Fisica*, the annual educational and training course for high school teachers, as well as several initiatives for high school students, like *Masterclasses, Inspyre International School, Students in Staff* and the *Summer School,* many of which can be performed as work-related learning projects.

Finally, for the general public, a *Visitor Center* was realized in building 29 in 2017. This is our first space completely dedicated to the external public. Here detector prototypes and other illustrative material of the research activities will be exposed for didactical purposes.

We would like to sincerely thank the whole LNF staff for making it possible to achieve these results.

EVENTS 2017	PARTICIPANTS
Visits for kids, high school and university students	2300
OpenLabs for the general public	2500
Seminars and Public Lectures (at the LNF and outside)	4900
IDF and IDFM ("Incontri di Fisica") for high school teachers	237
Stages for high school students	376
"Matinées di scienza" for high school students	830
Career Day	530

Table 1 Overview of outreach events organized at LNF during 2017.

LNF in numbers

The LNF personnel, at the end of 2017, consists of 322 units, including 60 with a fixed term contract, plus 206 associate members. Among these, there are university and PhD students, young post-Docs and employees from universities or other research institutions. Associate members work alongside staff members and likewise take part in the laboratory's activities. Tab. 1 shows the division of the LNF personnel among the different profiles.

	Staff	Temp.	Tot.
Researchers	67	6	73
Engineers	41	24	65
Administrative employees	28	10	38
Technicians	126	20	146
Tot.	262	60	322

Distribution of LNF collaborators years 2017

- Employes
- Italian associates [LNF+CS]
- Foreign associates [LNF+CS]
- Italian users
- Foreign users

Table 1 LNF personnel at December 2017